Titre: Title:	Stemless InSb nanowire networks and nanoflakes grown on InP
Auteurs: Authors:	Marco Rossi, Teun A. J. van Schijndel, Pim Lueb, Ghada Badawy, Jason Jung, Wouter H. J. Peeters, Sebastian Kölling, Oussama Moutanabbir, Marcel A. Verheijen, & Erik P. A. M. Bakkers
Date:	2024
Type:	Article de revue / Article
Référence: Citation:	Rossi, M., van Schijndel, T. A. J., Lueb, P., Badawy, G., Jung, J., Peeters, W. H. J., Kölling, S., Moutanabbir, O., Verheijen, M. A., & Bakkers, E. P. A. M. (2024). Stemless InSb nanowire networks and nanoflakes grown on InP. Nanotechnology, 35(41), 415602 (11 pages). https://doi.org/10.1088/1361-6528/ad61ef

Stemless InSb nanowire networks and nanoflakes grown on InP

Marco Rossi[1], Teun A.J. van Schijndel[1,2], Pim Lueb[1], Ghada Badawy[1], Jason Jung[1], Wouter H.J. Peeters[1], Sebastian Kölling[3], Oussama Moutanabbir[3], Marcel A. Verheijen[1,4] and Erik P.A.M. Bakkers[1]*.

[1)] Applied Physics and Science Education Department, Eindhoven University of Technology, 5600 MB Eindhoven, The Netherlands

[2)] Electrical and Computer Engineering, University of California Santa Barbara, Santa Barbara, CA 93106, USA.

[3)] Department of Engineering Physics, École Polytechnique de Montréal, Montreal, Québec, Canada.

[4)] Eurofins Materials Science Netherlands B.V., High Tech Campus 11, 5656 AE Eindhoven, The Netherlands

* Corresponding author: e.p.a.m.bakkers@tue.nl

Supplementary information

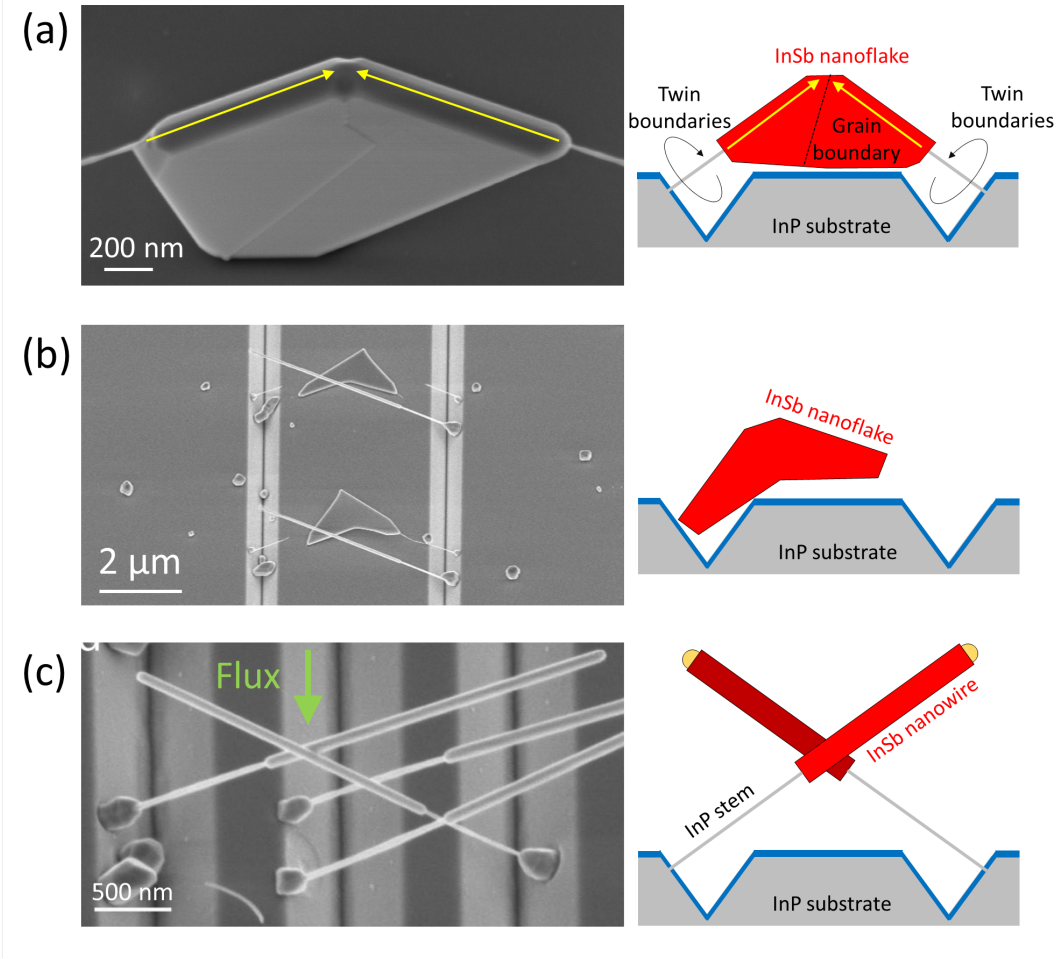

Figure S1 – Downsides of Growing Interconnected InSb Nanowires on Intermediary Stems. Examples are provided by using an InP platform with inclined {111}B facets ("trenches") and InP-InAs stems to induce nanowire merging, as developed in the previous work at reference[1]. Each example includes a side-view SEM image with a simplified sketch. (a) An InSb nanoflake resulting from the merging of two InSb nanowires (indicated by yellow arrows) with a visible grain boundary. Grain boundaries form as InSb nanowires grow on stems with multiple twin boundaries orthogonal to the growth direction. (b) Two InSb nanoflakes that have fallen on the substrate due to stem evaporation during InSb growth. Fallen InSb nanostructures cannot be used for any device fabrication purpose. (c) Nanowires grown adjacent to each other allow the fabrication of semiconductor-superconductor hybrid devices with an abrupt junction. This is achieved by exploiting the inter-shadowing effect between the nanowires during a directional superconductor deposition parallel to the trenches (green arrow). However, junctions created on the stems are useless for Majorana-Zero-Modes (MZMs) experiments. Furthermore, junctions created close to the edges of the InSb nanowires do not provide enough space for gate connections. The SEM image was retrieved from reference[2].

SI.1 - Substrate fabrication and nanowire growth details

InP(111)B substrate. The fabrication starts from an out-of-the-box InP(111)B 2-inch wafer. The native oxide is removed by wet etching in a H_3PO_4:H_2O 1:10 solution. A 20 nm thin layer of SiN_x is deposited by using plasma-enhanced physical vapor deposition (PECVD). The adhesion promoter AR 300-80 is spun at 4000 rpm for 60 s and baked for 2 min at 180°C. The positive resist AR-P 6200.04 is spun at 4000 rpm for 60 s and baked for 3 min at 150°C. Circular nanoholes with varying pitch are patterned using electron-beam-lithography (EBL). After resist development in AR 600-546 and rinsing in IPA, two methods for nanohole fabrication within the SiN_x mask are tested: one set of samples undergoes a dry etching process utilizing a reactive-ion etching of CHF_3 and oxygen plasma (for 20 seconds), while another set undergoes wet etching using a buffered hydrofluoric acid (BHF) solution (NH_4F:HF 7:1) for 13 seconds. A 8 nm thin layer of Au is deposited on both sets of samples by electron-beam physical vapor deposition, followed by resist lift-off using PRS-3000, leaving Au only in the nanoholes. The sample is ready for the nanowire growth.

InP(100) substrate with trenches. The fabrication starts from an out-of-the-box InP(100) 2-inch wafer. The procedure for fabricating inclined {111}B facets follows the same steps as the publication at reference[1]. After the fabrication of trenches, the steps required for patterning the selective-area mask follow the same recipe as used for the InP(111)B substrate, employing dry etching technique for nanohole cavity fabrication.

Nanowire growth. The following bullet point list provides a summary of the parameters employed in the MOVPE growth runs of stemless InSb nanowires on InP substrates. The growth scheme is illustrated in figure 1b of the main text. The MOVPE reactor has a total volume of 6000 liters and is kept at a constant pressure of 50 mbar.

- Growth runs with AsH_3 heat-up. The AsH_3 molar fraction during the heat-up step is varied between $4.33\cdot10^{-3}$ and $8.33\cdot10^{-3}$ between different runs. For the nucleation, AsH_3 removal, and growth steps, the TMIn molar fraction ranges from $2.09\cdot10^{-7}$ to $5.02\cdot10^{-7}$, and the TMSb molar fraction varies from $8.26\cdot10^{-5}$ and $1.67\cdot10^{-3}$ in different runs. The growth temperature is varied between 495°C to 510°C, and the growth step time between 90 minutes and 120 minutes in distinct growth runs. Cooldown: all the growth runs TMSb = $1.12\cdot10^{-3}$.
- Growth run with PH_3 heat-up (Figure 1d). Heat-up: $PH_3 = 6.67\cdot10^{-3}$. Nucleation / remove group-PH_3 / InSb growth step (90 min): TMIn = $3.49\cdot10^{-7}$, TMSb = $7.10\cdot10^{-4}$, Cooldown TMSb = $1.12\cdot10^{-3}$.
- Growth run with TMSb heat-up (Figure 1c). Growth scheme at reference[3] applied on our InP(111)B substrate with dry etched nanoholes. Heat-up: TMSb = $1.12\cdot10^{-3}$. InSb growth step (180 min): TMIn = $3.49\cdot10^{-7}$, TMSb = $6.35\cdot10^{-4}$, Cooldown under TMSb = $1.12\cdot10^{-3}$.

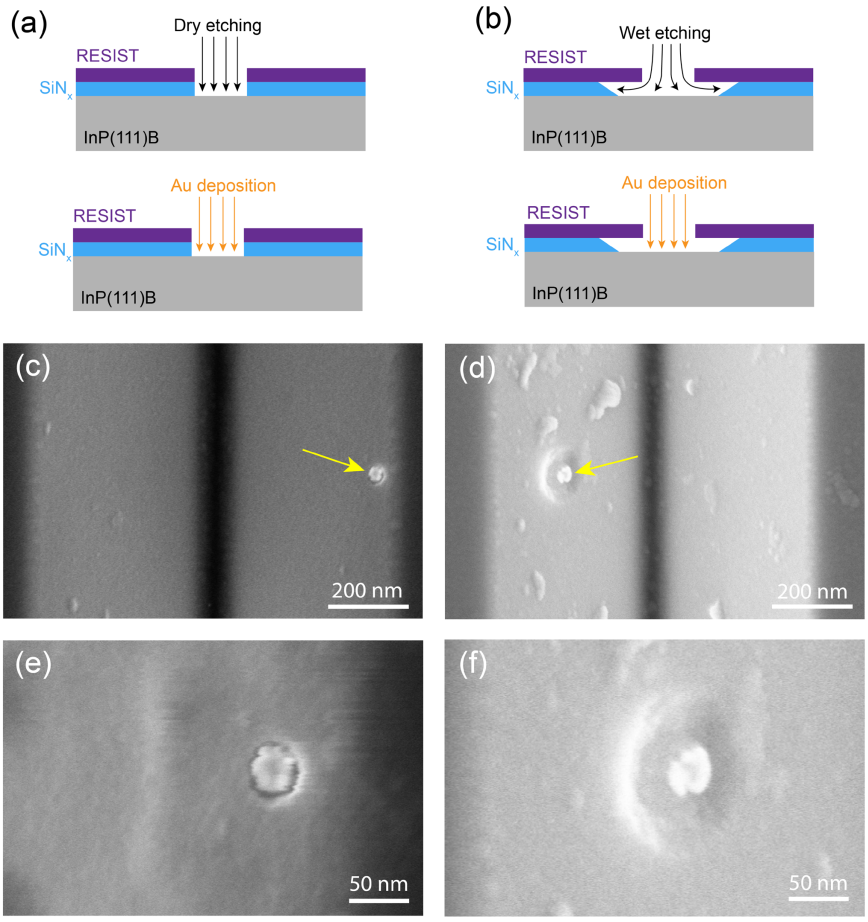

Figure S2 – Comparison between dry-etched and wet-etched nanoholes in the SiN_x mask. (a,b) Schematic illustrations of the two different processing steps used to fabricate the substrates for nanowire growth. A positive electron-beam lithography resist is spun onto the sample, patterned with circular nanoholes, and developed. (a) Dry etching is directional and removes the SiN_x mask only below the patterned opening in the resist. The subsequent directional Au deposition completely fills the exposed area of the InP substrate. (b) Wet etching is isotropic, thus areas of the SiN_x mask that are covered by resist are removed. The subsequent directional Au deposition leaves part of the InP unexposed both to Au or SiN_x. (c-f) Top-view SEM images of (c) a dry-etched nanohole and (d) a wet-etched nanohole, both containing Au droplets of the same diameter (marked by yellow arrows) fabricated on trenches of an InP substrate. Images (e) and (f) show a magnified view of (c) and (d), respectively, highlighting the different morphology of the nanohole cavity provided by the two etching techniques.

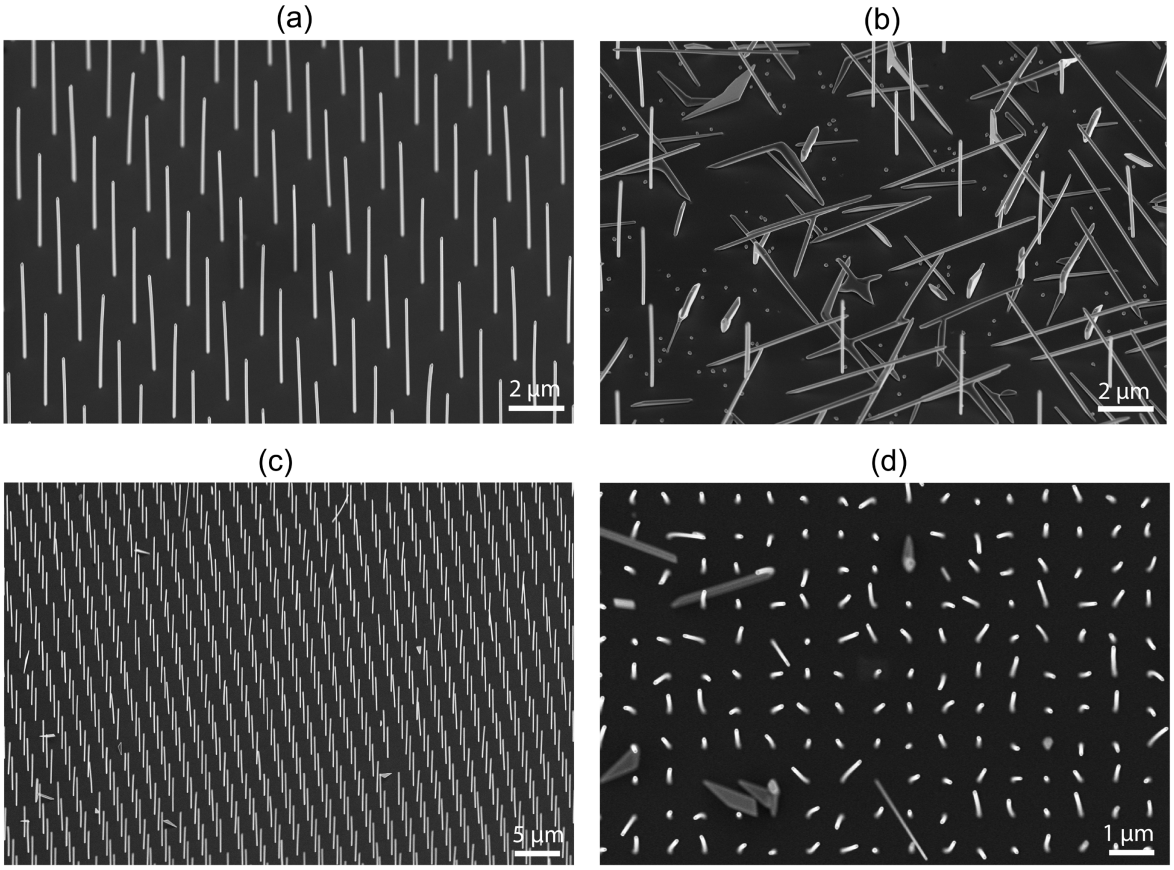

Figure S3 – (a,b) Representative tilted-view SEM images of InSb nanowires grown on InP(111)B substrate using an AsH_3 heat up before InSb growth. Comparison between a substrate with (a) dry etched and (b) wet etched nanoholes. (c) Overview image of (a), demonstrating high yield of vertical growth. Pictures (a-c) were taken with the stage tilted by 30°. (d) Representative top-view SEM image highlighting the bending behavior of the nanowires grown from dry etched nanoholes.

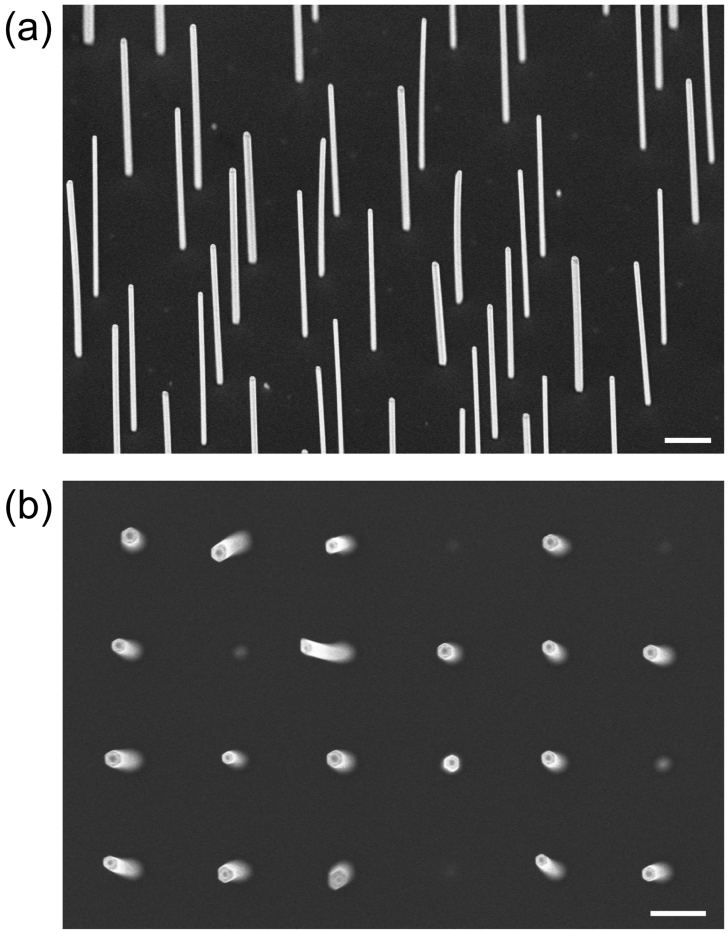

Figure S4 – (a) Tilted view and (b) top view SEM images of stemless InSb nanowires grown on a InSb(111)B substrate with a AsH3 heat up step. The nanowires display a bending behavior similarly to stemless nanowires grown on InP(111)B with an AsH3 heat up step. The scale bar in (a) is 1 µm, while in (b) is 400 nm.

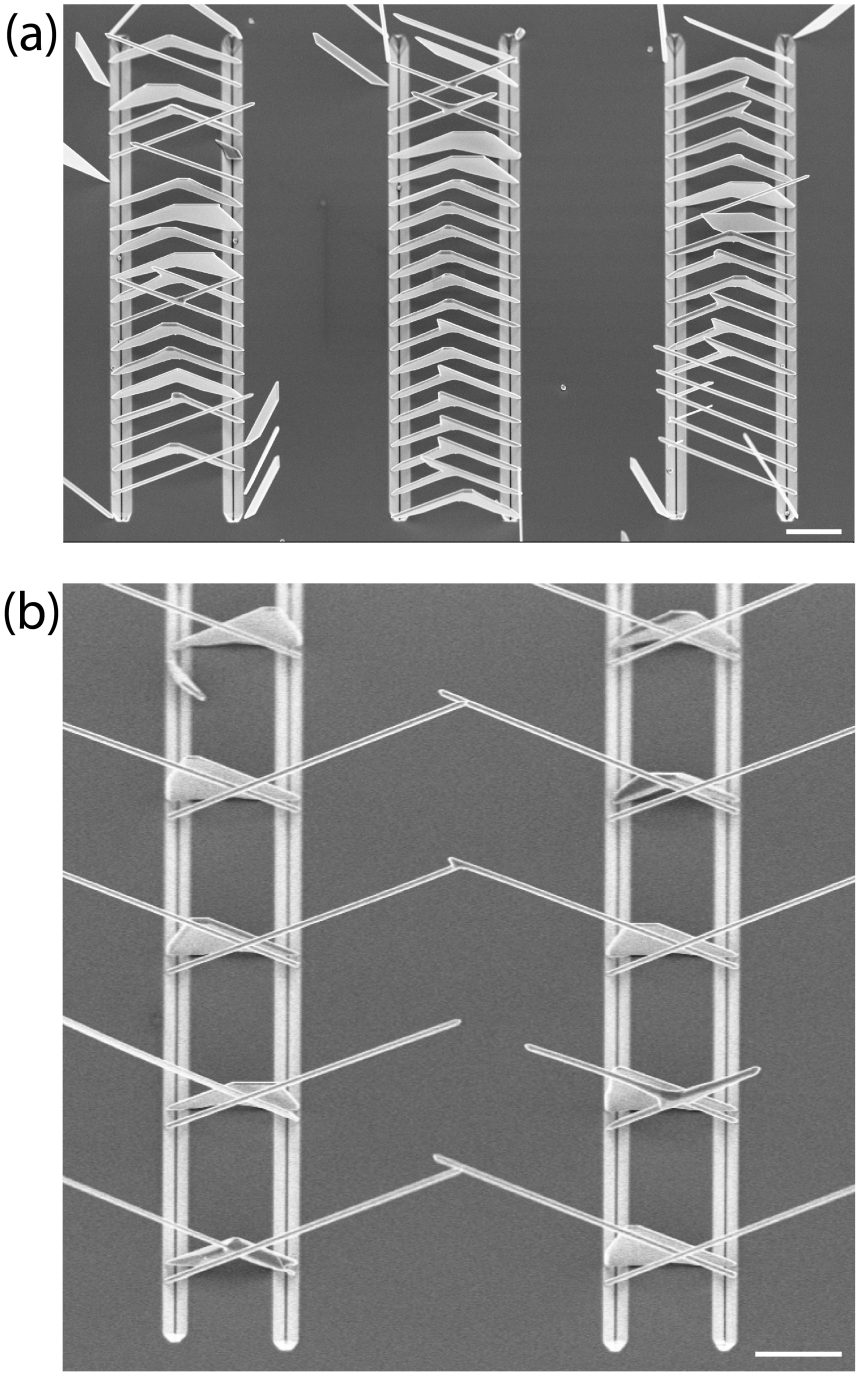

Figure S5 – (a) series of stemless InSb nanoflakes intentionally grown on InP trenches. Pair of Au droplets are deposited with an offset Δy=0 on opposing trenches and stemless InSb are grown, leading to a merging event in most of the cases. Nanoflakes and nanobridges display the characteristic trapezoidal morphology that indicates the absence of grain boundaries[1]. (b) Overview image of shadowing designs where two crossing nanowires are intentionally grown in front of a InSb nanoflake. The nanoflakes show the characteristic trapezoidal morphology. Only two nanoflakes developed into a 3D bulky nanostructure. Scale bars are 2 μm.

SI.2 – Statistical analysis of nanowire bending

The curvature of nanowires grown using an AsH_3 heat-up step is estimated by visually inspecting SEM images of nanowire fields. The primary goal is to calculate the mean curvature of nanowires within the same field to enable comparisons with other fields. Additionally, the mean curvatures can be compared with the theoretical predictions given by the bending model. The calculation of the mean curvature of a field requires to determine the curvature of a statistically significant number of nanowires. However, manually determining the curvature of individual nanowires is impractical due to their varying bending directions. To overcome this problem, we have developed an SEM image-recognition software capable of automating the measurement of various nanowire dimensions (e.g., length and thickness) for each nanowire displayed in an SEM picture. Moreover, we have established a method to estimate the nanowire curvature using certain approximations, as will be explained in detail below.

The starting approximation of our method is that all the nanowires are bent following the trajectory of an arc of a circle. Therefore, each nanowire has a curvature radius r that determines the extent of their bending (see figure S6a). The measurement of the curvature radius of a nanowire enables to calculate the curvature, which is defined as its inverse:

$$K \equiv \frac{1}{r} \qquad (1)$$

The curvature radius of nanowires can be measured following a two-steps process using the image recognition software, where the sample is imaged with the SEM stage tilted at two distinct angles. In both imaging perspectives, the software can identify all nanowires within an SEM image and measuring their straight-line distance from base to tip. These measurements enable to determines the distances L and δ, defined as illustrated in figure S6a, which are then used to calculate r.

To measure L, a side-view image of a field of nanowires is captured, with the SEM stage tilted at an angle β with respect to the electron beam of the microscope. An example of a SEM image with β=10° is shown in figure S6b, which also illustrates the sample's orientation in relation to the electron beam. The software automatically determines the straight-line distance between the base and tip of each nanowire from the viewpoint of the image (p in figure S6b). Knowing the tilting angle of the SEM stage, L can be calculated using the formula:

$$L = \frac{p}{\sin\beta} \qquad (2)$$

It is important to mention that the measured p of each nanowire varies depending on the point of view because the nanowires captured in the SEM picture display different out-of-plane bending directions. Therefore, formula *(2)* provides an approximate value for L. However, considering that the nanowires exhibit only a slight deviation from growing in a perfectly straight direction (i.e. $r >> L$), we consider negligible any error arising from the estimation of L due to these different bending orientations of the nanowires in a picture. Moreover, under the same consideration, L can be reasonably regarded as a good estimation of the nanowire's length.

To measure δ, the SEM stage is tilted to β=0°, and a top-view SEM image of the same field is taken. The software measures the straight-line distance between the base and tip of each nanowire, as well as their thickness (q and t in figure S6c, respectively). For each nanowire, we calculate the distance δ as:

$$\delta = q - t \qquad (3)$$

Subtracting the nanowire thickness t from q is particularly important to correctly detect unbent nanowires, since q is measured by the software as the largest pixel-to-pixel distance of a detected object. In case of bent nanowires, we consider equation *(3)* to be a valid approximation for the determination of δ since nanowires display only slight curvatures, making the nanowire tip extension as viewed from top-view close to the nanowire thickness. Therefore, the calculation of δ using equation *(3)* is an approximation meant to exclude the contribution of the nanowire tip extension from the extent of the bending measured from the top view. The radius of curvature of each nanowire in the top-view picture can be calculated using geometrical considerations (see figure S6a):

$$r = \frac{L}{2\cos\gamma} \tag{4}$$

where:

$$\gamma = \cos^{-1}\left(\frac{\delta}{L}\right) \tag{5}$$

Tracking individual nanowires becomes complex when transitioning from a sideview perspective ($\beta \neq 0$) to a top view ($\beta = 0$) in SEM imaging of fields. This complexity makes it impossible to measure both L and δ for each nanowire within a field. To address this, we first calculate the mean nanowire length $<L>$ of the field of nanowire from sideview imaging and then we use it to estimate the curvature radius of each nanowire in the top-view image with equations *(4)* and *(5)*. We consider this a valid approximation as the nanowire length distributions are narrow (see Figure S7). The curvature K of each nanowire in the top-view SEM picture is calculated using this formula:

$$K = \frac{1}{r} = \frac{2\delta}{<L>^2} \tag{6}$$

Curvature distributions for fields of nanowire having different pitch can be plotted using this formula (see figure S9). The mean curvature and spread are extracted from these plots by fitting each distribution with a two-parameter distribution.

The measurement of curvature using this method is affected by a systematic error that arises from the sample clamping procedure on the SEM stage before imaging. To clamp the sample with nanowires, a piece of carbon tape is manually adhered to the SEM stage, and the sample is then sticked to it using tweezers. Subsequently, the sample is loaded into the SEM vacuum chamber for imaging. However, samples manually attached in this manner do not always lie perfectly flat on the SEM stage with respect to the ebeam source, introducing a systematic in the detection of δ during top-view imaging of nanowires. Due to the imperfect clamping, the orientation of all the nanowire tips shifts in the same direction and by the same extent with respect to the electron beam. This introduces a constant offset in all the detected δ. The systematic error becomes evident when imaging straight InSb nanowires, i.e. those grown without using AsH_3 and in an As-free reactor, as they appear apparently curved. Figures S8a-c display three representative top-view SEM images of the same field of straight nanowires, captured during different SEM sessions where the carbon tape was replaced before clamping the sample each time. It is clear from the images that all the nanowire tips lean towards the same direction in every image, marked by the colored arrows, but the direction varies among the three SEM sessions.

A quantitative proof of the occurrence of the imperfect sample clamping is provided by applying the SEM image recognition software to the top-view SEM images of the same field retrieved during the three SEM sessions. The software can determine the angle at which every detected object is oriented with respect to the xy-coordinate system of the SEM image, as defined by the scale bar and the direction perpendicular to it. The software fits an ellipse around every detected nanowire to enclose their area, thus determining a major and minor axis. We note that imaged nanowires typically have brighter tips

and darker bottoms, thus we instruct the software to consistently fit ellipses by orienting their major axis from the darker to the brighter side. The orientation angle towards each detected object lean is defined as the angle formed between the major axis of the ellipse and the xy-coordinate system of the SEM image. All the orientation distributions are narrow but centered at different angles among the three plots, demonstrating that the sample is clamped imperfectly on the SEM stage and with different tilts between the three SEM sessions. The smaller peaks visible in figures S8d and S8e are artifacts from the SEM imaging process. They arise because a minority of nanowires have darker tips and brighter bases, which leads to detected orientations with a 180-degree offset in comparison to nanowires displaying brighter tips and darker bases.

We can use our established method for the curvature calculation to estimate the extent of apparent curvature. The procedure explained in figure S6 is applied to the straight InSb nanowires grown without using AsH_3 imaged during the three SEM sessions. Figure S8g-i display the curvature distributions resulting from this analysis, showing that nanowires have a comparable mean curvatures and standard deviations in the three sessions. If we calculate the average between the mean curvatures among the three sessions, we obtain a value of $2.7 \cdot 10^{-6}$ nm^{-1} with standard deviation $5.8 \cdot 10^{-7}$ nm^{-1}, providing an indication of the extent of the systematic error.

The orientation and curvature study were conducted on bent InSb nanowires grown using AsH_3, and the results for field of nanowires having different pitch are presented in Figure S9. In contrast to As-free nanowires, those grown using AsH_3 exhibit orientation spectra that encompass the entire angular spectrum (figures S9a-d). Interestingly, a broad peak centered approximately at 90° and a dip at a 180-degree orientation offset from it are consistently observed in all orientation spectra. The curvature distributions are depicted in Figures S9e-h, revealing that most of the nanowires have much higher curvatures compared to the apparent curvature values due to the systematic error in sample clamping. The mean curvatures of bent nanowires are 2 to 3.5 times higher than our estimated average apparent curvature. Furthermore, the curvature distributions of bent nanowires have spreads (σ in the figures) that are 3.6 to 7.6 times greater than the standard deviation of the apparent curvature. Therefore, the occurrence of systematic error when imaging of bent nanowires cannot be overlooked but has a minor impact on the determination of mean curvatures and spreads. Additionally, these findings suggest that the broad peak centered around 90° in the orientation spectra of all the nanowires grown using AsH_3 (Figure S9a-d) may be attributed to a preferential bending orientation. However, confirming this statement and finding the underlying causes of this phenomenon requires further experiments, which are not explored in this study.

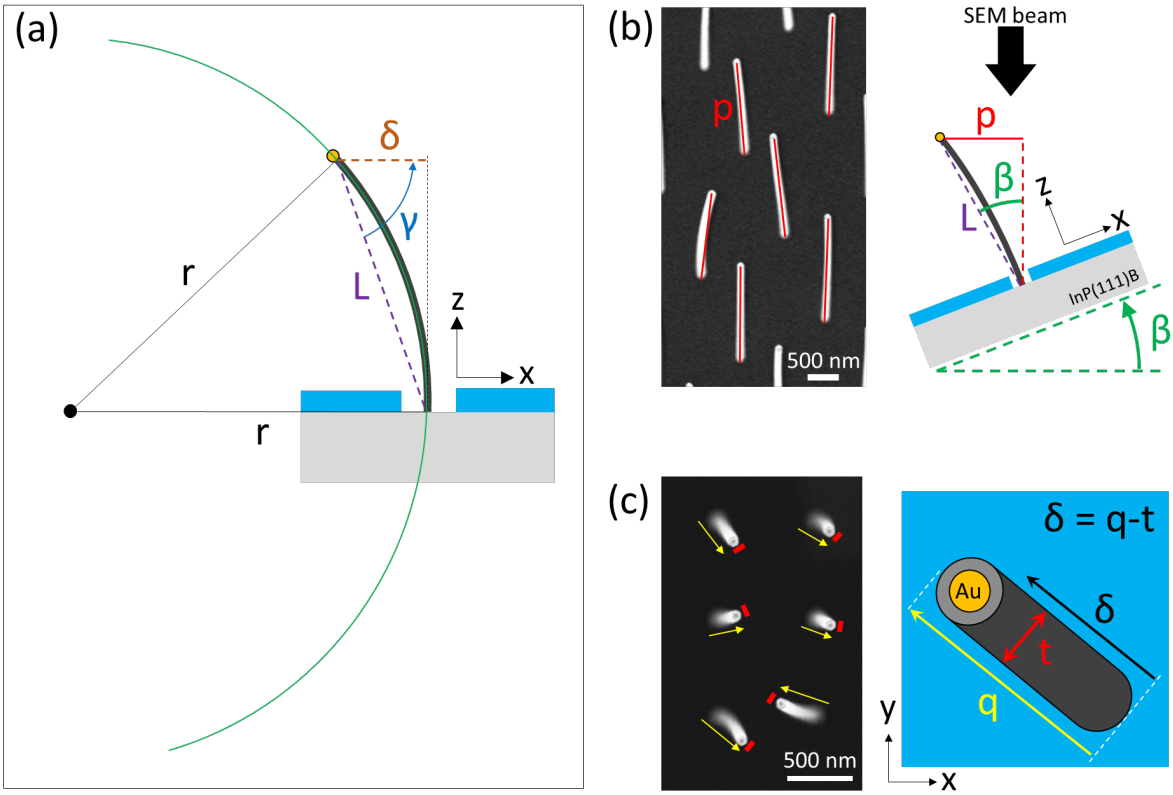

Figure S6 – (a) Sketch of the model used to estimate the bending of nanowires grown using AsH_3 with the SEM image-recognition software. The nanowires are assumed to be bent following an arc of a circle with a radius of curvature *r*, where the inverse gives the nanowire curvature. The curvature radius can be estimated by measuring *L* and *δ* following a two-step procedure sketched in figures (b) and (c). (b) The SEM stage is tilted to an angle *β*=10° and the software automatically retrieve the straight-line distances *p* between base and tip of all the nanowires. A good approximation of the distance *L* can be calculated from *p* knowing *β*, considering negligible the slightly different out-of-plane bending orientations of the nanowires. (c) The SEM stage is tilted to *β*=0° to image the nanowires from top view. The software automatically measures the straight-line distance *q* and the thickness *t* of every nanowire. The formula *δ*=*q*-*t* is used as an approximation to determine δ for each nanowire, and it is meant to exclude the contribution of the nanowire tip extension from the extent of the bending.

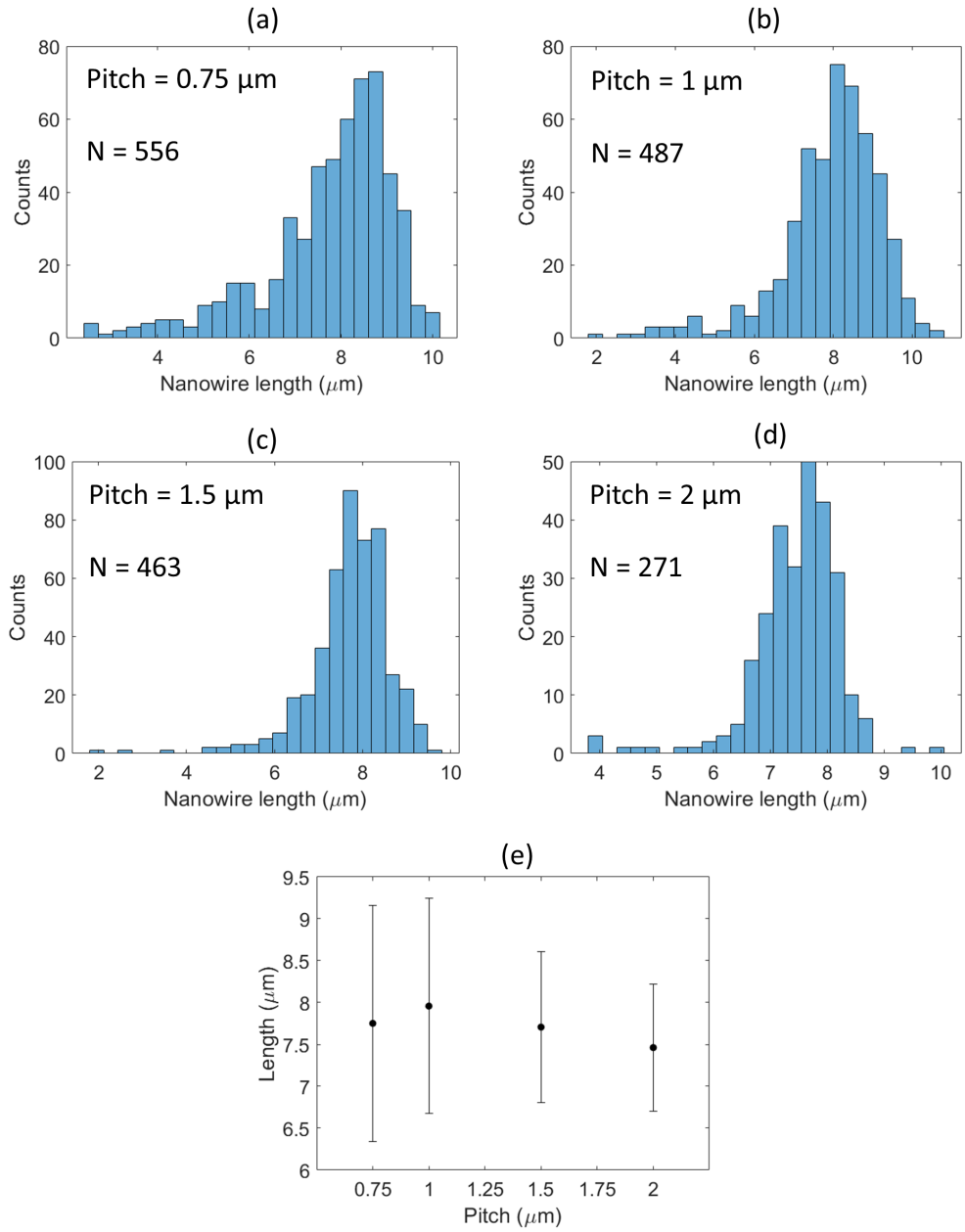

Figure S7 – (a-d) Distribution of nanowire lengths for fields of nanowires with different pitches on the same InP substrate. The sample was prepared using a SA mask with dry-etched nanoholes and grown using an AsH_3 heat-up process. The distributions were obtained using the SEM image recognition software. Each distribution reports the pitch of the imaged field and total number of measured nanowires (N). (e) Plot of the nanowire length as a function of the pitch. The data points are the mean values of the distributions (a-d) and error bars given by the standard deviations.

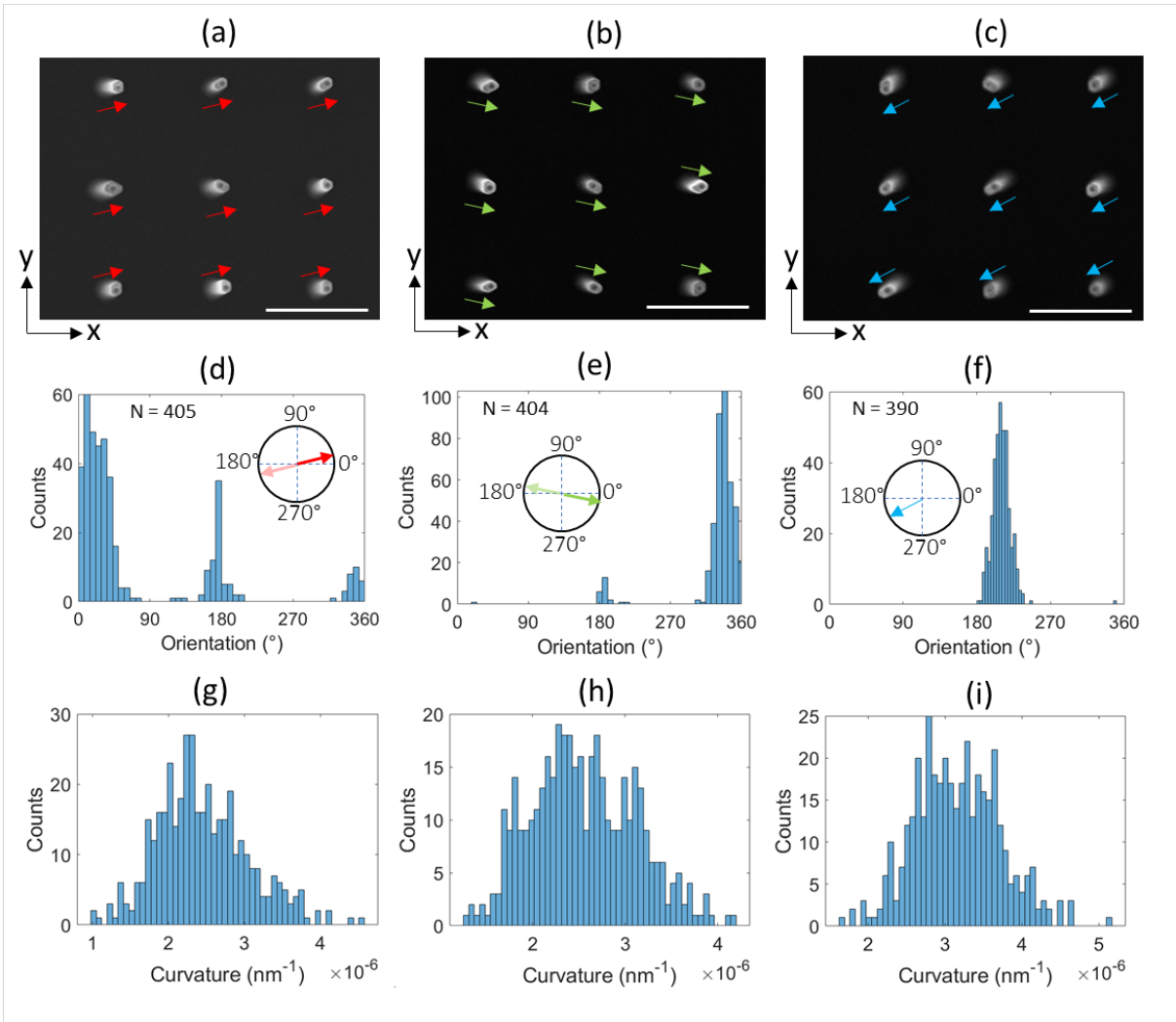

Figure S8 – Extent of the systematic error due to the imperfect sample clamping procedure on the SEM stage. Unbent, stemless InSb nanowires grown without using AsH_3 were imaged consecutively in three steps. Before each imaging step, the sample with nanowire is unclamped and clamped again on the SEM stage. (a-c) Representative top-view SEM images of the same field of nanowire after each clamping step, showing nanowire tips pointing all in the same direction due to misalignment of the sample on the SEM stage. The misalignment is different after each clamping and marked by the colored arrows. The scale bars are 1 µm. (d-f) Histograms showing the nanowire tip orientations of the same field of nanowires after each clamping, retrieved using image recognition software. The insets highlight the average orientation of the nanowire tips in each plot. A small fraction of nanowires tip may be counted with a 180-degree orientation offset, even though their tips are directed in the same direction as the other nanowires, and it is an artifact resulting from the programming of the software. N is the number of imaged nanowires. (g-i) Apparent curvature distributions of the analyzed nanowires from (d-f), respectively, resulting from the imperfect clamping procedure. The mean apparent curvature C and standard deviation σ of these distributions are: (g) $C=2.45\cdot10^{-6}$ nm^{-1}, $\sigma=6.0\cdot10^{-7}$ nm^{-1}, (h) $C=2.54\cdot10^{-6}$ nm^{-1}, $\sigma=5.6\cdot10^{-7}$ nm^{-1}, (i) $C=3.18\cdot10^{-6}$ nm^{-1}, $\sigma=5.7\cdot10^{-7}$ nm^{-1}.

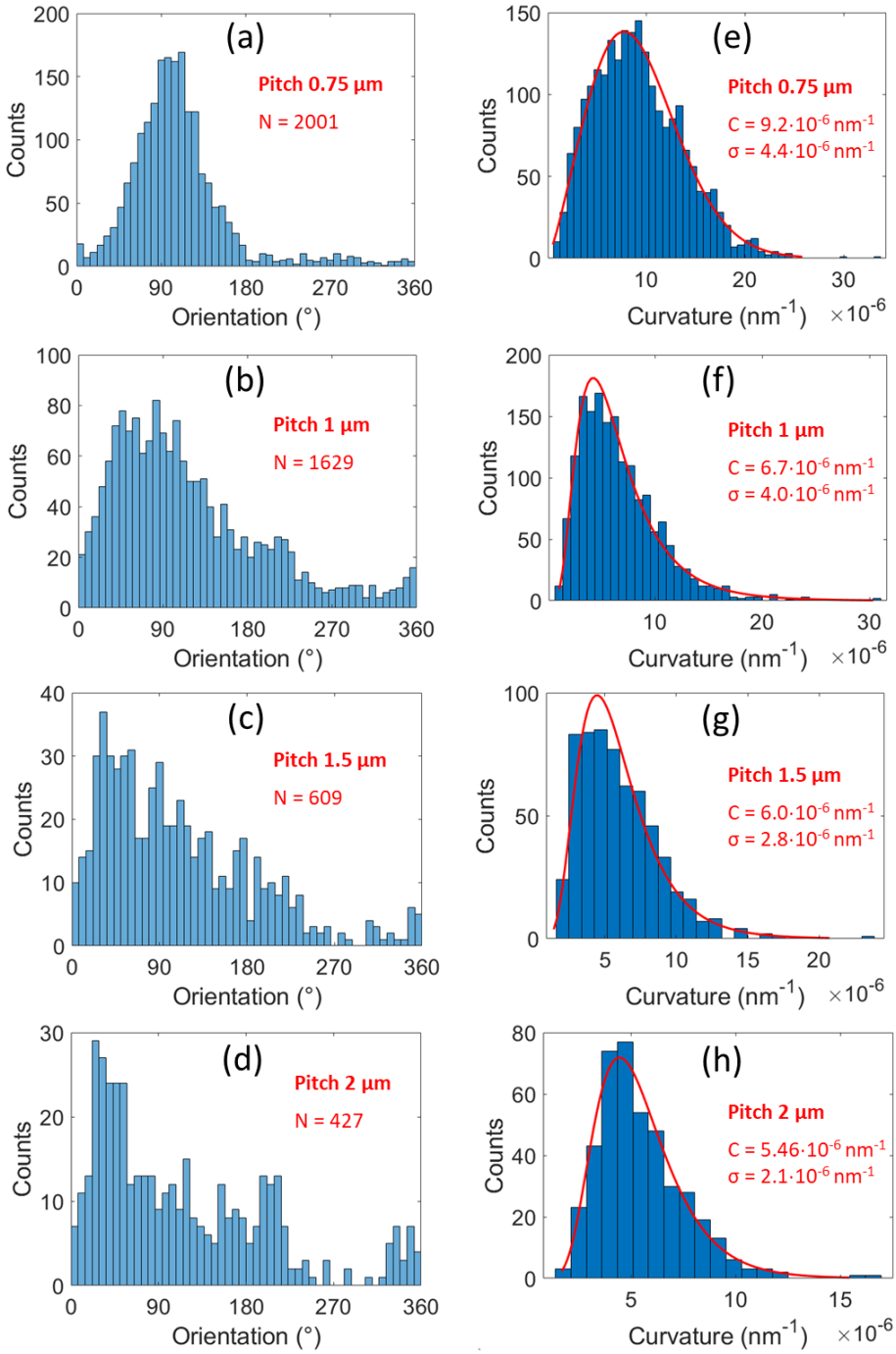

Figure S9 – Statistical analysis results obtained using the image-recognition software. A representative sample of bent, stemless InSb nanowires grown on InP(111)B using AsH_3 during heat-up was analyzed. The histograms in (a-d) display the distribution of nanowire tip orientations for fields with different pitches when imaged from a top-view. N is the number of imaged nanowires. (e-f) Curvature distributions of the fields of nanowires of analyzed in (a-d), respectively. Each distribution is fitted (red lines in the plots) by a two-parameter distribution, i.e. Burr distribution for (e) and lognormal for (f-h), whose mean (C) and variance (σ^2) is calculated. The square root of the variance is taken as error bar for the curvature for the plots shown in figures 2f and 3c of the main text.

SI.3 – Bending model details

The bending model is based on the continuum elasticity theory and follows the same approach described in the supplementary information of the work by Lewis, R.B. et al[4]. In this section, we offer a summary of the approach employed in this prior work, adapted to the framework of our study case.

The nanowire cross-section is modeled as described in figure 3b of the main text. Strain in the nanowire arises due to the presence of an asymmetric $InAs_xSb_{1-x}$ core-shell alloy with two different lattice constants of core and shell. The expression for the strain energy per unit length along the axis of the nanowire is:

$$U = \frac{1}{2}\int E\,\varepsilon^2 dA \qquad (7)$$

Here, E is the Young's modulus, ε the strain, and dA represents an infinitesimal area element within the cross section of the nanowire. The integral is calculated over the entire nanowire cross section. Only the component of the strain parallel to the axial direction of the nanowire is considered in this analysis. Assuming that the nanowire is constrained to remain straight and that the core-shell interface is coherent, the core and shell regions share the same lattice constant at their interface ($a_{interface}$) along the entire length of the nanowire, leading to strain in these regions given by:

$$\varepsilon_{core} = \frac{a_{interface} - a_{core}}{a_{core}} \qquad (8)$$

$$\varepsilon_{shell} = \frac{a_{interface} - a_{shell}}{a_{shell}} \qquad (9)$$

In these equations, a_{core} and a_{shell} are the unstrained lattice constants of the core and shell, respectively, in the axial direction of the nanowires and given by applying Vegard's law[5]. The As molar fractions, x_{core} and x_{shell}, used to calculate a_{core} and a_{shell}, respectively, with Vegard's law are indicated in figure 3b and are the average values of those measured in the cross-sectional STEM-EDX study indicated in figure S13. By introducing the strains of equations *(8)* and *(9)* into equations *(7)*, we can write an expression for the strain energy U in the case of the nanowire constrained to remain straight:

$$U_{straight} = \frac{1}{2}\left(E_{core}\varepsilon_{core}^2 A_{core} + E_{shell}\varepsilon_{shell}^2 A_{shell}\right) \qquad (10)$$

Here, A_{core} and A_{shell} are the cross-sectional areas of the hexagonal-shaped core and the asymmetric shell, respectively, which are defined by the geometry of our nanowire cross-section shown in figure 3b of the main text. The expression of the lattice constant at the core-shell interface for the case of the straight nanowire can be found by minimizing equation *(10)* with respect to $a_{interface}$:

$$a_{interface,\ straight} = \frac{a_{core}a_{shell}(a_{core}A_{shell}E_{shell} + a_{shell}A_{core}E_{core})}{a_{core}^2 A_{shell}E_{shell} + a_{shell}^2 A_{core}E_{core}} \qquad (11)$$

If we remove the assumption that the nanowire is constrained to be straight, strain along the nanowire axis can be relieved by nanowire bending. Continuity of the lattice parameter along the axial direction of the nanowire is still required at the core-shell interface. In this scenario, the strain varies linearly along the x-axis that bisects the nanowire into two symmetric sections, as depicted in the sketch in figure S10. The strain is given by:

$$\varepsilon_{core} = \frac{a_{interface} - a_{core}}{a_{core}} + \frac{x}{r} \quad for\ x < |R_x| \qquad (12)$$

$$\varepsilon_{shell} = \frac{a_{interface} - a_{shell}}{a_{shell}} + \frac{x}{r} \quad for\ x \geq |R_x| \tag{13}$$

where r is the radius of curvature of the nanowire and R_x coordinate of the core-shell interface along the x-axis (see figure S10). Assuming that the strain components depend solely on x, the expression for the strain energy per unit length along the nanowire axis is:

$$U = \frac{1}{2}\int \left[E_{core} w_{core}(x)\varepsilon_{core}^2(x) + E_{shell} w_{shell}(x)\varepsilon_{shell}^2(x)\right]dx \tag{14}$$

In this equation, $w_{core}(x)$ and $w_{shell}(x)$ are the widths of the core and shell, respectively, at coordinate x as sketched in figure S10, and where:

$$w_{shell}(x) = w_{total}(x) - w_{core}(x) \tag{15}$$

The curvature radius of the nanowire can be calculated by minimizing equation *(14)* with respect to r, assuming $E_{core}=E_{shell}$ and $a_{interface}=a_{interface,straight}$. Subsequently, the nanowire curvature is calculated using equation *(1)*.

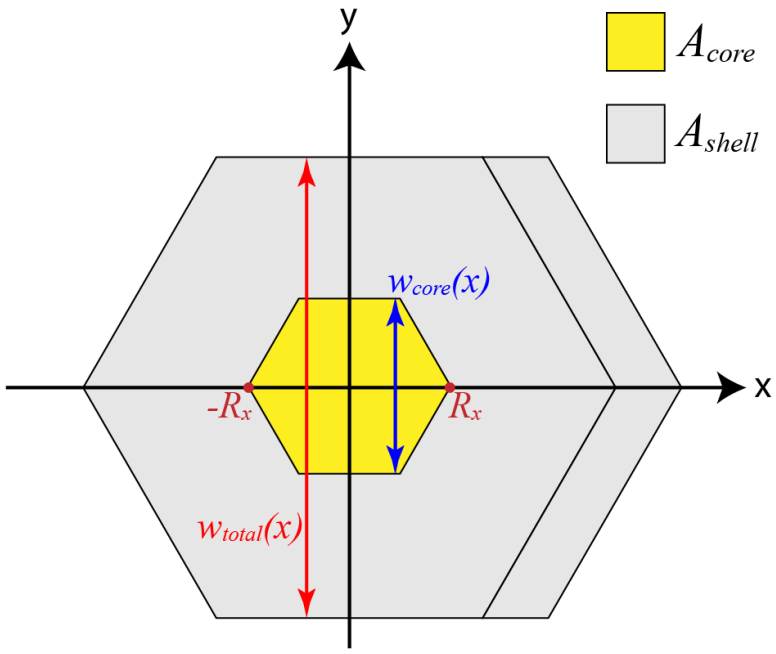

Figure S10 – Schematic illustration of the nanowire cross-section used to compute the strain in the bending model.

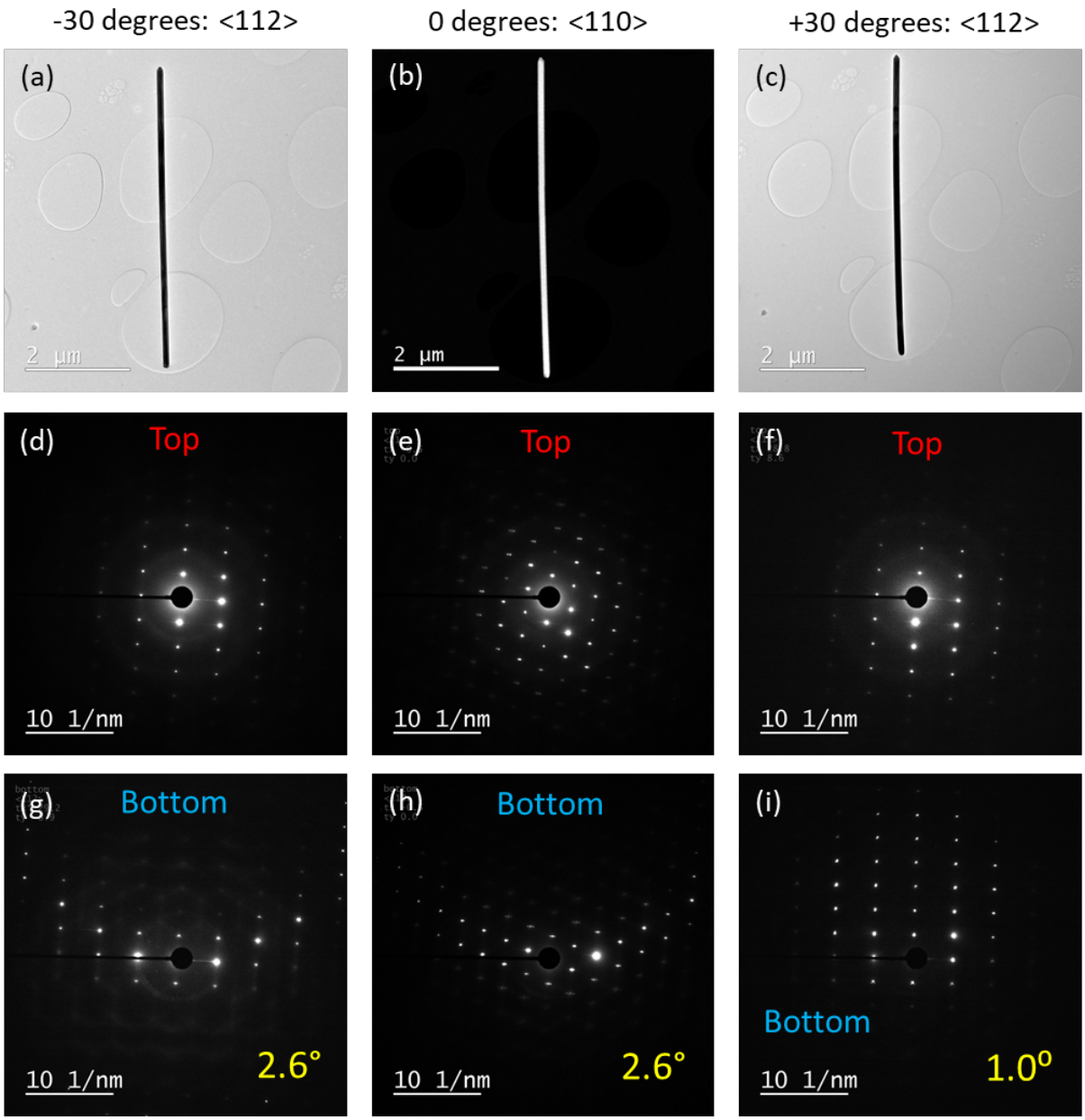

Figure S11 – TEM study of a representative InSb nanowire grown on InP using an AsH_3 heat up. The nanowire displayed bending on the growth substrate and was mechanically transferred using a nanomanipulator onto a holey carbon film for the TEM inspection. (a,c) bright field TEM images and (b) High-angle annular dark-field scanning transmission electron microscopy (HAADF-STEM) image of the same transferred nanowire imaged along 3 different zone axes (differing by their rotation along the long axis of the nanowire). For every zone axis, the top of the nanowire was aligned exactly on zone axis and the electron diffraction patterns were acquired from (d-f) the top and (g-i) the bottom, showing single-crystalline zincblende diffraction patterns. The bottom diffraction patterns are tilted with respect to the top diffraction patterns due to nanowire bending. The numbers in yellow in (g-i) give the additional tilts that were needed to rotate the bottom part back to the zone axes.

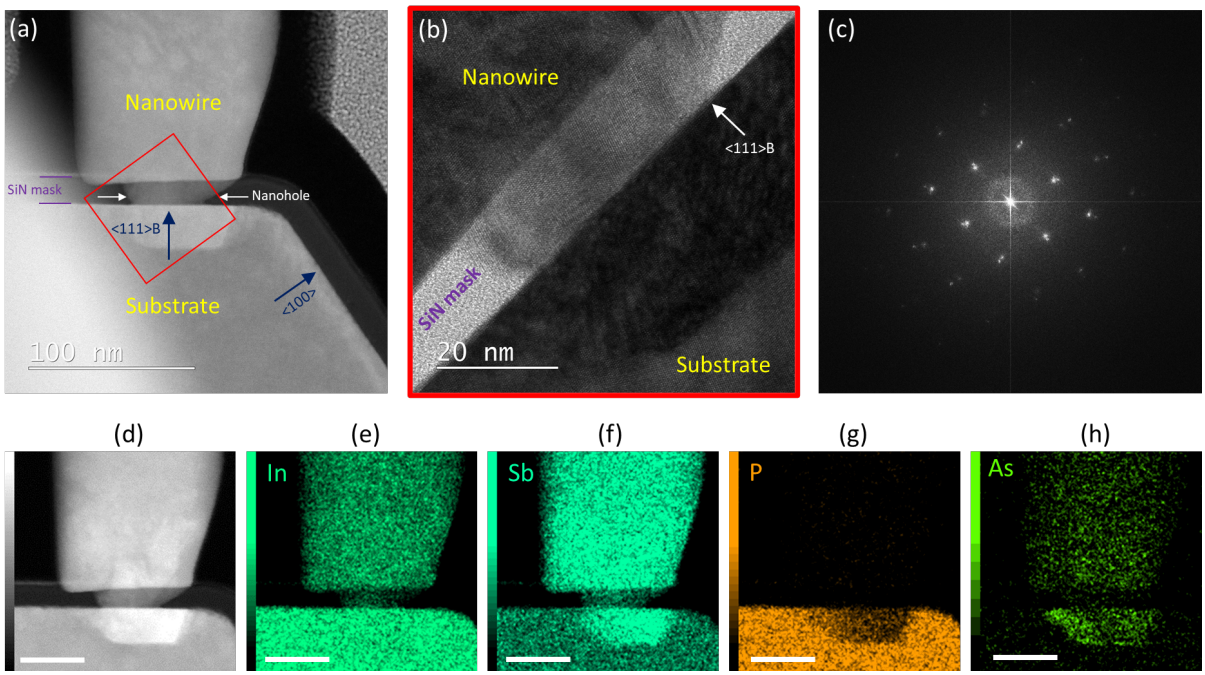

Figure S12 – Cross-sectional TEM analysis of the base of a stemless InSb nanowire grown on an inclined {111}B facet of an InP(100) substrate. (a) HAADF-STEM image of the cross-sectional sample, showing the substrate and the nanowire base. (b) HR-TEM image of the interface between the substrate and the nanowire, and (c) its corresponding Fast-Fourier transform (FFT) pattern. The pattern shows double spots for each reciprocal lattice vector, implying that the nanowire has an epitaxial relation to the substrate and that the nanowire lattice is relaxed, i.e. it displays another periodicity than the substrate. (d-h) EDX study of the interface between the substrate and the nanowire. The elemental mapping demonstrates that the nanowire base is mostly made of indium (In) and Sb, with evident incorporation of As impurities. Below the nanohole cavity of the SiN_x mask, a region of approximately 40 nm within the InP substrate shows P depletion and Sb and As enrichment. The presence of Sb in the rest of the substrate is an artifact due to the overlap of the peaks of In and Sb in the EDX spectrum. Scale bars in (d-h) are 50 nm.

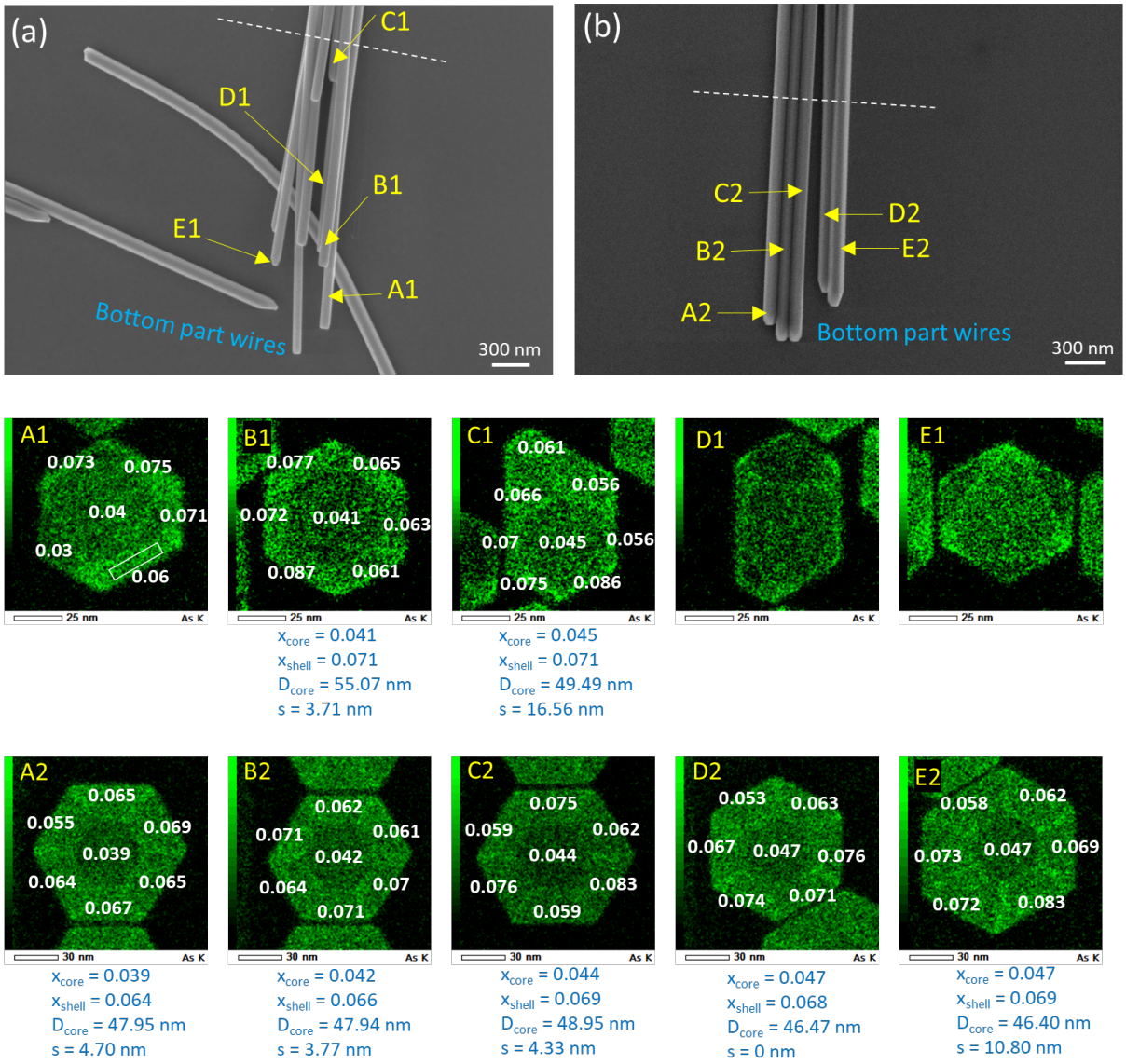

Figure S13 – (a,b) Top view SEM images of a group of InSb nanowires after mechanical transfer to a bare wafer for TEM lamella preparation. These nanowires belong to the field with pitch of (a) 0.75 µm and (b) 2 µm of the same growth sample. The nanowires were grown on an InP substrate using an AsH_3 heat-up step. The cross-sectional samples were made at the white dashed lines. Quantified EDX mappings of the As content in each nanowire cross-section are displayed below the SEM images. Considering an $InAs_xSb_{1-x}$ alloy, the numbers indicate the local As fraction x, highlighting that 8 out of 10 nanowires (A1-C1 and A2-E2) exhibit a core-shell structure, characterized by an As-poor core and an As-rich shell. The accuracy in percentage As for areas selected within the EDX mapping is approximately 0.5 at%. Thus, the As molar fraction has an error of ~0.008. Not all the nanowires have the same cross-sectional shape, since the six {110} nanowire side facets do not have the same width, leading to a distorted hexagon in many cases. Input parameters for the bending model are displayed below each As mapping. Geometrical parameters (D_{core}, s) are retrieved by overlapping regular hexagons with a thickening s on each core-shell map (see white lines of figure 3a in the main text). The As fractions x_{core} and x_{shell} are the As fractions measured in the core and the average As fraction of the shell, respectively. Parameters are not retrieved from nanowire A1 since its core is not fully surrounded by an As-rich shell.

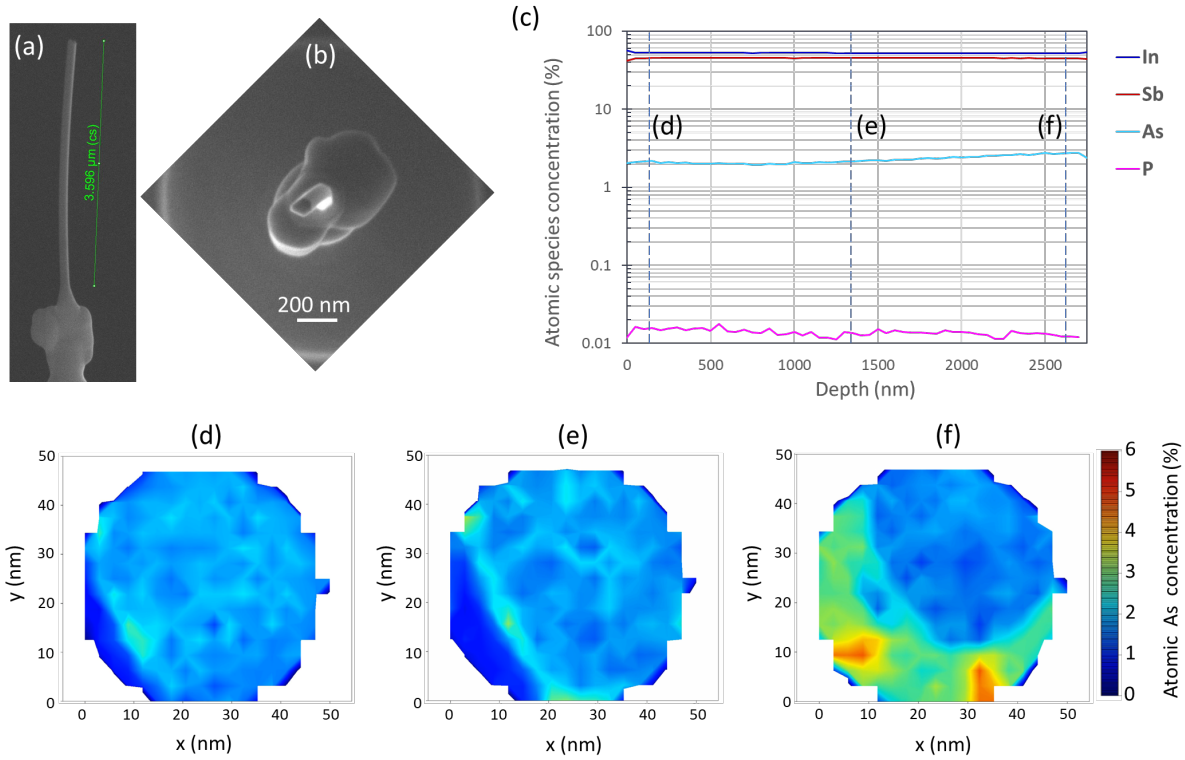

Figure S14 – Atom probe tomography (APT) analysis of a bent nanowire. (a) Side view and (b) top view SEM images of the analyzed bent nanowire. (c) The nanowire tip is at 0 nm depth. The nanowire is made of In and Sb, with As and P present as impurity along the entire length. The detected concentration of the III-V species deviates from the 50:50 stoichiometry likely due to the occurrence of experimental errors in the APT procedure[6]. The cross-sectional As maps at different nanowire heights are shown in figures (d-f), corresponding to the nanowire heights marked by the dashed lines in figure (c). Figures (d-f) reveal the presence of As incorporation with different local As atomic concentrations along each nanowire cross-sectional map. The cross-sectional mapping is limited to a cylinder with a diameter of 50 nm, while the nanowire has a maximum thickness of about 110 nm. Therefore, the APT analysis is limited to the central part of the nanowire cross-section, likely displaying only the VLS-grown core and a small part of the VS-grown shell. The As atomic concentrations can be compared to the As molar fractions (displayed in figure S13) by dividing the latter by 2, as the atomic concentration accounts for the indium content, which constitutes 50% of the atomic composition of the nanowire, while the As molar fractions are related only to the group-V species. Accordingly, the As molar fractions can be compared with the As atomic concentrations by multiplying the latter by 2. The average arsenic atomic concentration vs depth, displayed in figure (c), varies from 3% near the base to 2% towards the tip. These values are consistent with the As molar fraction within the VLS core of the nanowires quantified by EDX (see figure S13), which ranges from x=0.039 (atomic As concentration = 1.95%) and x=0.047 (atomic As concentration = 2.35%).

Bibliography

1. Rossi, M. *et al.* Merging Nanowires and Formation Dynamics of Bottom-Up Grown InSb Nanoflakes. *Adv. Funct. Mater.* **33**, 2212029 (2023).

2. Op het Veld, R. L. M. InSANe InSb nanowire quantum devices - PhD Thesis, Eindhoven University of Technology. (2021).

3. Badawy, G. *et al.* High Mobility Stemless InSb Nanowires. *Nano Lett.* **19**, 3575–3582 (2019).

4. Lewis, R. B. *et al.* Nanowires Bending over Backward from Strain Partitioning in Asymmetric Core-Shell Heterostructures. *Nano Lett.* **18**, 2343–2350 (2018).

5. Denton, A. R. & Ashcroft, N. W. Vegard's "law". *Phys. Rev.* **43**, 3161 (1991).

6. Riley, J. R. *et al.* Atom probe tomography of a-axis GaN nanowires: Analysis of nonstoichiometric evaporation behavior. *ACS Nano* **6**, 3898–3906 (2012).